ACS Catalysis

Research Article

pubs.acs.org/acscatalysis

Acid-Functionalized SBA-15-Type Periodic Mesoporous Organosilicas and Their Use in the Continuous Production of 5-Hydroxymethylfurfural

Mark H. Tucker,[†,∥] Anthony J. Crisci,[‡,∥] Bethany N. Wigington,[‡] Neelay Phadke,[†] Ricardo Alamillo,[†] Jinping Zhang,[§] Susannah L. Scott,*[,‡,⊥] and James A. Dumesic*[,†]

[†]Department of Chemical and Biological Engineering, University of Wisconsin, Madison, Wisconsin 53706-1607, United States

[‡]Department of Chemistry & Biochemistry, University of California, Santa Barbara, Santa Barbara, California 93106-9510, United States

[§]Suzhou Institute of Nano-Tech and Nano-Bionics, Chinese Academy of Science, Suzhou, China 215125

[⊥]Department of Chemical Engineering, University of California, Santa Barbara, Santa Barbara, California 93106-5080, United States

Supporting Information

ABSTRACT: The activity, selectivity, and stability of several supported acid catalysts were evaluated in tubular reactors designed to produce 5-hydroxymethylfurfural (HMF) continuously from fructose dissolved in a single-phase solution of THF and H_2O (4:1 w/w). The reactors, packed with the solid catalysts, were operated at 403 K for extended periods, up to 190 h. The behaviors of three propylsulfonic acid-functionalized, ordered porous silicas (one inorganic SBA-15-type silica, and two ethane-bridged SBA-15-type organosilicas) were compared with that of a propylsulfonic acid-modified, nonordered, porous silica. The HMF selectivity of the catalysts with ordered pore structures ranged from 60 to 75%, whereas the selectivity of the nonordered catalyst under the same reaction conditions peaked at 20%. The latter was also the least stable, deactivating with a first-order rate constant of 0.152 h^{-1}. The organosilicas are more hydrothermally stable and maintained a steady catalytic activity longer than the inorganic SBA-15-type silica. The organosilica with an intermediate framework ethane content of 45 mol % was more stable, with a first-order deactivation rate constant of only 0.012 h^{-1}, than the organosilica containing 90 mol % ethane linkers in the framework. The catalysts were recovered and characterized after use by ^{13}C and ^{29}Si solid-state NMR, elemental analysis, nitrogen adsorption/desorption, X-ray diffraction, and SEM/TEM. Deactivation under flow conditions is caused primarily by hydrolytic cleavage of acid sites, which can be (to some) extent recaptured by the free surface hydroxyl groups of the silica surface.

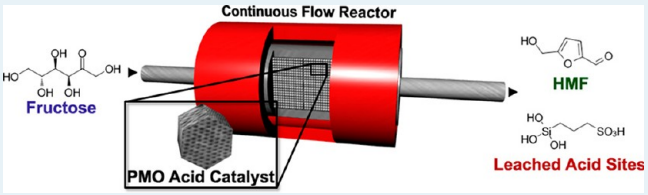

KEYWORDS: *5-hydroxymethylfurfural, continuous dehydration, packed-bed reactor, SBA-15, periodic mesoporous organosilicas, propylsulfonic acid, catalyst deactivation rate*

INTRODUCTION

The conversion of biomass to value-added chemicals is a rapidly growing research area.[1] In particular, HMF has been identified as a potential platform chemical for the production of carbohydrate-derived chemical feedstocks, fuels, and materials.[2−15] Currently, HMF is produced most efficiently by the acid-catalyzed dehydration of fructose. Both homogeneous catalysts (e.g., mineral acids,[16] organic acids,[17] Lewis acids such as $CrCl_2$ and $AlCl_3$,[18,19] ionic liquids[20]) and heterogeneous (solid acid) catalysts[21,22] are active. Heterogeneous acid catalysts are desirable because they tend to be less corrosive, easier to separate, and more readily adapted to large-scale, continuous production. Furthermore, flow reactors containing a heterogeneous acid catalyst can, in principle, be used to couple dehydration with other reactions, even when the coupled reactions are acid-sensitive. For example, glucose, a less expensive feedstock, may be catalytically isomerized to fructose prior to dehydration,[23] and HMF may be oxidized, reduced, or esterified[2,24] downstream from its synthesis, avoiding the need for its isolation.

The production of HMF in batch reactors is well-documented,[15,25−28] but there are relatively few reports on its continuous production.[29−34] The continuous dehydration of mono- and polysaccharides to HMF was reported in a biphasic solvent system using titania or zirconia as the catalyst.[29] Although the titania deactivated, it was regenerated by calcination (the regeneration of the zirconia catalyst was not discussed). Unfortunately, the rate of HMF production was not reported as a function of time-on-stream, so the rates of deactivation are unknown. H-mordenite was tested in a

Received: May 14, 2012
Revised: July 8, 2012
Published: July 9, 2012

continuous pilot plant reactor; however, catalyst stability was not reported.[30,31] Several niobia-based catalysts were employed for the dehydration of aqueous fructose in a fixed-bed reactor.[32,33] Mixed silica−niobia oxides showed stable activity for ∼95 h on-stream at 373 K, despite coke formation, although HMF selectivity was low (<15%, at fructose conversions from 15 to 35%). The dehydration of fructose in DMSO was studied using a cation-exchange resin as the catalyst.[34] High catalyst stability was reported, with a stable HMF yield even after 900 h on-stream. However, since the reaction was conducted at high fructose conversion, it does not allow for accurate assessment of catalyst stability.

Developing active and robust solid acid catalysts for aqueous reactions is important not only for the production of HMF but also for other transformations, such as transesterification and hydrolysis, that are critical to the conversion of biomass to valuable chemical intermediates. The stability of solid acid catalysts has not yet been evaluated for catalysts that achieve high HMF selectivity. In particular, silica-supported acid catalysts are known to give high activity and selectivity, but the studies were conducted batch-wise.[35,36] Under hydrothermal reaction conditions, the anchored acid sites are often unstable, and it is difficult to exclude the possibility that homogeneous acids are also capable of promoting the reaction. Consequently, it is necessary to study supported catalysts in a flow reactor to accurately assess their activity (e.g., in comparison to the activity of homogeneous catalysts) as well as to understand the causes and rates of deactivation.

The hydrothermal stability of propylsulfonic acid-functionalized mesoporous-ordered silica catalysts depends on both the solvent system and the temperature.[37−40] The mesostructures of such materials have been reported to be stable for 24 h in boiling water,[38] while other studies show extensive loss of mesopore ordering after 48 h.[40] At 323 K, catalytic activity for the transesterification of acetic acid in water was retained over four reaction cycles, each lasting 24 h;[37] however, at 413 K in a water/toluene mixture, the activity declined by nearly 40% after just two cycles of 4 h duration each.[39] Loss of activity may be caused by cleavage of the active sites from the support, collapse of the silica mesostructure blocking access to the active sites, or deposition of insoluble reaction products in the pores.

Periodic mesoporous *organo*silicas (PMOs),[41] synthesized by condensation of organic-linker-bridged disilanes, $(RO)_3Si-R-Si(OR)_3$, have higher hydrothermal stabilities compared with mesoporous silicas with purely inorganic frameworks,[42] presumably because of their lower water affinity. Hydrophobicity and other chemical properties can be tuned by varying the organic group present in the hybrid organic−inorganic framework.[43] PMOs can be synthesized with a variety of mesostructures, including the *p6mm* geometry of SBA-15.[44] Propylsulfonic acid-functionalized PMO catalysts have also been prepared, either by co-condensation[45] or by postsynthesis grafting.[46]

In this work, the stabilities of silica- and organosilica-based catalysts were assessed under the demanding conditions typically required for efficient biomass conversion (elevated temperature and high water content). A series of propylsulfonic acid-modified silicas was explored, including a commercially available nonordered porous silica, an SBA-15-type ordered porous silica, and two ethane-bridged PMOs with SBA-15-type structures. Their activities were measured in packed-bed, continuous reactors. This approach permits a quantitative comparison of the extent of deactivation for different catalysts. The reactor configuration was found to be important because of the occurrence of liquid channeling and readsorption of cleaved active sites. After reaction, the catalysts were recovered and characterized to assess changes in their chemical and physical properties.

EXPERIMENTAL METHODS

Reagents and Materials. Tetraethyl orthosilicate (TEOS, 98%), tetramethyl orthosilicate (TMOS, 98%), 3-mercaptopropyltrimethoxysilane (MPTMS, 95%), 1,2-bis(trimethoxysilyl)-ethane (BTME, 96%), fructose (≥99%), and silica gel (high purity, pore size 6 nm, surface area 550 m^2/g, 70−230 mesh) were purchased from Aldrich and used as received. Pluronic P123 was obtained from BASF. Fused silicon dioxide (granular, 4−20 mesh), referred to below as SiO_2 chips, was purchased from Aldrich and was used as received or crushed before use, as noted. H_2O_2 (30 wt % in water) was purchased from EMD Chemicals. NaCl (Certified ACS Crystalline) and tetrahydrofuran (Certified) were obtained from Fisher Scientific. Ethanol (200 proof, Gold Shield) was used as received. Siliabond propylsulfonic acid (0.65 mmol/g) without end-capping (pSO_3H-SC) was purchased from SiliCycle, Inc. (Toronto, Canada). 3-(Trihydroxysilyl)-1-propanesulfonic acid in 30−35% water was purchased from Gelest. The acid site loadings of the synthesized catalysts were assumed to be equal to their sulfur contents as measured by elemental analysis.

The silica catalysts synthesized for this work were dried under vacuum (0.1 mTorr) at 423 K for 15 h and stored in an argon-filled glovebox prior to characterization. Prior to reaction studies, the catalysts were stored in a desiccator to prevent adsorption of atmospheric moisture. The pSO_3H-SC catalyst was used as received.

Characterization. Solid-state NMR spectra were recorded on a Bruker DSX500 WB spectrometer operating at 12.0 T, with frequencies of 125 and 99 MHz for ^{13}C and ^{29}Si, respectively. Samples were packed under argon into 4-mm zirconia rotors (Bruker). ^{29}Si magic angle spinning (MAS) and cross-polarization/magic angle spinning (CP/MAS) spectra were obtained using a 90° pulse length of 2.5 μs, a contact time of 5 ms, and high-power proton decoupling during detection. Typically, 25 000 scans were acquired at a spinning rate of 10 kHz. Chemical shifts were referenced using tetrakis-(trimethylsilyl)silane. ^{13}C CP/MAS spectra were obtained using a 90° pulse length of 2.4 μs, a contact time of 2 ms, and high-power proton decoupling during detection. Typically, 25 000 scans were acquired at a spinning rate of 10 kHz. Chemical shifts were referenced using adamantane.

Powder X-ray diffraction (XRD) patterns were collected from 0.6 to 4.0° [2θ], using a Panalytical MRD PRO diffractometer with Cu Kα radiation (0.02° resolution). N_2 adsorption/desorption measurements were performed on a Micromeritics Tristar 3000 Porosimeter. SEM and TEM images were acquired using a Hitachi S-4800 microscope and a FEI G^2 T20 microscope, respectively. Elemental analysis was performed by Columbia Analytical (Tuscon, AZ).

Synthesis of Propylsulfonic Acid-Functionalized PMO (E90). Following a modified literature procedure,[40] Pluronic P123 (1.91 g) was dissolved with stirring in 1.60 M aqueous HCl (70 mL), then heated to 318 K in a tightly sealed HDPE bottle (200 mL) in an oil bath. BTME (4.85 mL, 19.3 mmol) was added, followed 15 min later by NaCl (0.462 g). After a further 15 min, MPTMS addition was initiated (400 μL total, 100 μL aliquots over the course of 1 h). After 3 h, H_2O_2 (30 wt

dx.doi.org/10.1021/cs300303v | ACS Catal. 2012, 2, 1865−1876

%, 1.26 mL) was added to the reaction mixture. After 24 h, the reaction mixture was removed from the oil bath and divided equally among four 25 mL Parr pressure reactors equipped with Teflon liners. The reactors were placed in an oven at 373 K for 24 h. The resulting four suspensions were filtered, and each was washed with ~200 mL of water. The surfactant was removed by ethanol extraction; the solid was suspended in 500 mL of acidified ethanol (containing 2 M HCl) and refluxed for 24 h, then filtered and washed with ~200 mL of ethanol. The ethanol extraction was performed three times. The resulting solids were washed with ~200 mL deionized H_2O then suspended in 2 M HCl and stirred overnight. The solids were filtered and washed with H_2O until the pH of the filtrate was neutral. Finally, the organosilica was dried in air at room temperature overnight, then at 373 K under vacuum (0.1 mTorr) for 12 h. ^{13}C CP/MAS NMR: δ (ppm) 5 ($SiCH_2CH_2Si$), 12 ($SiCH_2$), 16 ($SiOCH_2CH_2$), 18 ($CH_2CH_2SO_3H$), 54 (CH_2SO_3H), 59 ($SiOCH_2CH_2$), 70 (P123). ^{29}Si MAS NMR: δ (ppm) −50 (T^1), −58 (T^2), −67 (T^3). Elemental analysis C: 18.91%, S: 1.69%, Si: 17.08%.

Synthesis of Propylsulfonic Acid-Functionalized PMO (E45). The same procedure for the synthesis of E90 was used, except that TMOS (1.38 mL, 9.36 mmol) and BTME (2.42 mL, 9.62 mmol) were used. They were combined prior to addition of NaCl. ^{13}C CP/MAS NMR: δ (ppm) 5 ($SiCH_2CH_2Si$), 12 ($SiCH_2$), 16 ($SiOCH_2CH_2$), 18 ($CH_2CH_2SO_3H$), 54 (CH_2SO_3H), 59 ($SiOCH_2CH_2$), 70 (P123). ^{29}Si MAS NMR: δ (ppm) −58 (T^2), −67 (T^3), −100 (Q^3), −110 (Q^4). Elemental analysis C: 14.45%, S: 2.29%, Si: 19.79%.

Synthesis of Propylsulfonic Acid-Functionalized SBA-15 (E0). The same procedure for the synthesis of E90 was used, except that TEOS (4.31 mL, 19.3 mmol) was used instead of BTME. ^{13}C CP/MAS NMR: δ (ppm) 11 ($SiCH_2$), 18 ($CH_2CH_2SO_3H$), 54 (CH_2SO_3H;), 70 (P123). ^{29}Si MAS NMR: δ (ppm) −67 (T^3), −100 (Q^3), −110 (Q^4). Elemental analysis C: 5.25%, S: 3.50%, Si: 42.51%.

General Procedures for Continuous Fructose Dehydration. All reactors were well-insulated and were heated using electric heating tape (Cole-Parmer) located around the catalyst bed as well as the tubing leading to the reactor to preheat the liquid feed stream. In all cases, the catalysts were loaded into the reactors as free-flowing powders. The temperature was maintained at 403 K using a PID controller (Love Controls), a variable transformer (Tesco), and a K-type thermocouple (Omega). The liquid feed (2 wt % fructose in a solvent of 4:1 (wt/wt) THF/Milli-Q water) was pumped from a graduated cylinder into the reactor using an HPLC pump (Lab Alliance, series 1) at a constant rate. The reactor was pressurized with 200 psig He (Airgas). The pressure was controlled using a back pressure regulator (GO) and was monitored by gauges located before and after the catalyst bed. The reactor effluent was collected in a gas−liquid separator. The HPLC pump was turned off during reactor sampling. To keep the pressure constant, a valve located at the reactor outlet was closed during sampling, and the separator was repressurized with He before resuming operation. After each experiment, the reactor was cooled, then flushed with ~100 mL 4:1 (w:w) THF/Milli-Q water to remove physisorbed material. The catalyst was dried in the reactor at 373 K under flowing He (Airgas), followed by drying overnight in a vacuum oven (−24.5 in. Hg gauge pressure) at 383 K.

During the reaction, the product stream was analyzed using a Waters e2695 HPLC system, as described previously.[1] Fructose and HMF were analyzed using an Aminex HPX-87P column (Biorad) held at 358 K, with Milli-Q water as the mobile phase at a flow rate of 0.6 mL min^{-1}. Fructose concentration was monitored using a Waters 2414 refractive index detector, and HMF concentration was determined using a Waters 2998 photodiode array detector at 320 nm. Fructose conversion was calculated as moles of fructose reacted per mole of fructose fed. HMF selectivity was calculated as moles of HMF produced per mole of fructose reacted.

Continuous Fructose Dehydration in the 1/4 in. Simple Packed-Bed Reactor. In one configuration, used to qualitatively assess each catalyst, the reactor consisted of 1/4 in. o.d. stainless steel tubing, and the reaction was run up-flow (Figure 1a). On the basis of preliminary batch reactions (see

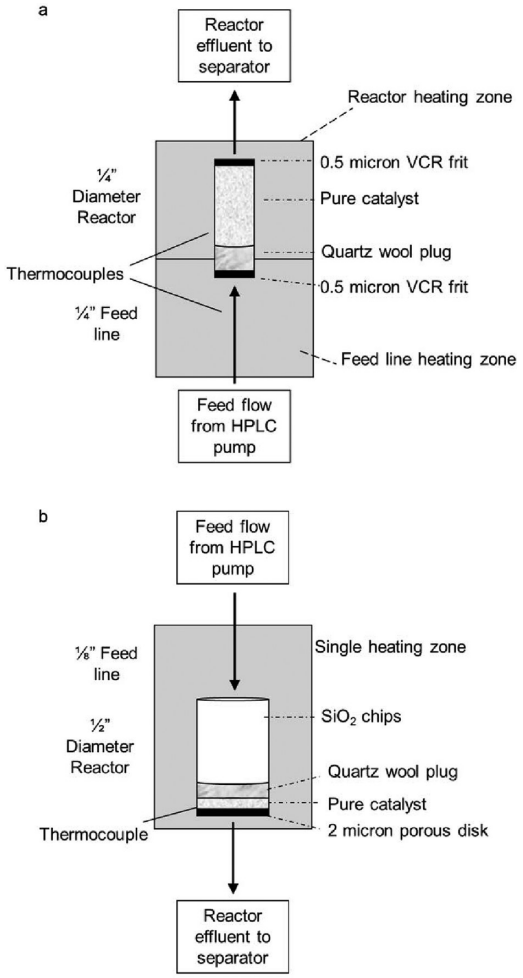

Figure 1. Schematic representations of (a) the 1/4 in. simple reactor, with a long catalyst bed held in place by fritted VCR fittings; and (b) the 1/2 in. simple reactor, with a short catalyst bed held in place by a porous glass disk.

Supporting Information), catalyst loadings of 0.267 g (E0), 0.311 g (E45), 0.346 (E90), and 0.330 g (pSO_3H-SC) were chosen to achieve similar, high fructose conversions in each case. Each catalyst was supported at the bottom by a plug of quartz wool (Grace), and packed tightly into the reactor. The top of the catalyst bed was held in place by a fritted VCR gasket (0.5 μm, Swagelok), which facilitated catalyst recovery for

dx.doi.org/10.1021/cs300303v | ACS Catal. 2012, 2, 1865−1876

Table 1. Physicochemical Properties of pSO_3H-Functionalized Catalysts[a]

catalyst	surface area, m^2/g		pore size,[b] nm		pore volume, cm^3/g		micropore volume, cm^3/g		H^+ content,[c] mmol/g
pSO_3H-SC	**660**	*282*	**4.3**	*4.9*	**0.79**	*0.44*	**0.054**		**0.65**
E0	**582**	*488*	**5.8**	*6.8*	**0.63**	*1.2*	**0.013**		**1.10**
E45	**559**	*604*	**4.5**	*4.6*	**0.55**	*0.77*	**0.082**	*0.014*	**0.71**
E90	**548**	*550*	**4.2**	*4.1*	**0.46**	*0.51*	**0.090**	*0.056*	**0.53**

[a]Bold and italic correspond to measurements made before and after catalyst use, respectively. [b]BJH pore diameter. [c]For pSO_3H-SC, the acid content was reported by the manufacturer. The acid contents for the mesoporous catalysts were calculated from S analysis. According to acid−base titration and XPS, in situ oxidation of MPTMS during catalyst synthesis is quantitative.[36]

postreaction characterization. The feed was delivered at a rate of 0.152 mL/min.

Continuous Fructose Dehydration in the 1/2 in. Simple Packed-Bed Reactor. In a second reactor configuration, designed to assess catalyst deactivation, the reactor consisted of 1/2 in. o.d. stainless steel tubing, and the reaction was run down-flow (Figure 1b). This reactor configuration minimizes channeling, due to the shorter length of the catalyst bed. The catalyst bed was supported by a 1/2 × 1/16 in. stainless steel porous disk (2 μm, McMaster-Carr) located between the end of the reactor tubing and a Swagelok fitting. The catalyst was packed tightly using a plug of quartz wool (Grace), and the remainder of reactor was filled with uncrushed SiO_2 chips to reduce the dead-volume in the reactor. The feed was delivered at a rate of 0.183 mL/min. To achieve a constant loading of acid sites (26.6 ± 0.2 μmol) in the reactor, the catalyst masses (derived from S elemental analysis) were adjusted as follows: 0.024 g (0E), 0.037 g (45E), 0.050 g (90E), and 0.041 g (pSO_3H-SC).

Continuous Fructose Dehydration in the Stacked Bed Reactor Configuration. To create the stacked bed reactor, the 1/2 in. reactor design and reaction conditions were replicated for each catalyst, with one modification: a bed of silica gel (0.122 g) was packed downstream and directly in contact with the catalyst bed (Figure 14). The 1/4 in. reactor design was similarly modified, but it was tested only with the pSO_3H-SC catalyst (Figure 15 (inset)). The catalyst bed (0.330 g) and silica gel bed (0.812 g) were separated by a plug of quartz wool so that both could be recovered at the end of the experiment and analyzed.

RESULTS AND DISCUSSION

Synthesis and Characterization of Propylsulfonic Acid-Functionalized Silica Catalysts. Three propylsulfonic acid-modified SBA-15-type silicas were synthesized by the co-condensation of 3-mercaptopropyltrimethoxysilane (MPTMS) with 1,2-bis(trimethoxysilyl)ethane (BTME) and/or a tetraalkoxysilane (either tetramethyl orthosilicate, TMOS, or tetraethyl orthosilicate, TEOS). For each material, 10 mol % of the Si in the synthesis mixture was derived from MPTMS. Framework Si was derived from a combination of the tetraalkoxysilane and BTME in various ratios. The catalysts are denoted 90E, 45E, and 0E, where the number refers to the mol % Si derived from BTME (i.e., 90, 45, and 0 mol %). In addition, a propylsulfonic acid-functionalized silica with a nonordered pore structure (pSO_3H-SC) was obtained from Silicycle.

The characterization of each synthesized material, reported in detail in the Supporting Information, is consistent with literature reports.[36,38,40] Physicochemical properties are summarized in Table 1. Nitrogen sorption analysis of the fresh catalysts produced type IV isotherms typical of mesoporous materials (Figure 2). Their BET surface areas and BJH pore diameters range from 575 to 650 m^2/g, and from 4 to 6 nm,

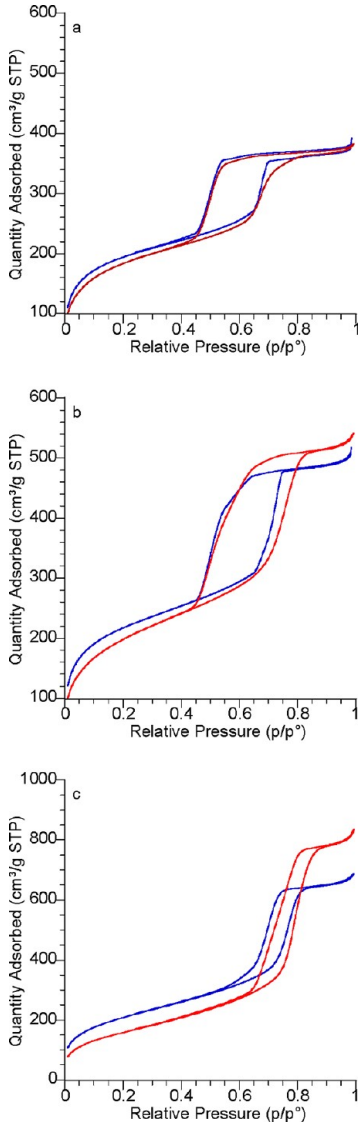

Figure 2. N_2 sorption isotherms for pSO_3H-SBA-15 catalysts: (a) E90; (b) E45; and (c) E0, before use in the dehydration reaction (blue) and after use on-stream (red) at 403 K. E90, E45, and E0 were on-stream for 60, 51, and 55 h, respectively.

respectively, consistent with other SBA-15-type materials. The *p6mm* mesostructure was confirmed by powder XRD. An intense, narrow peak near $2\theta = 1.00°$, common to all catalysts, is attributed to the d_{100} reflection (Figure 3). The d_{110} reflection also appears in each pattern near $2\theta = 1.60°$. For E0, the d_{200}

dx.doi.org/10.1021/cs300303v | ACS Catal. 2012, 2, 1865−1876

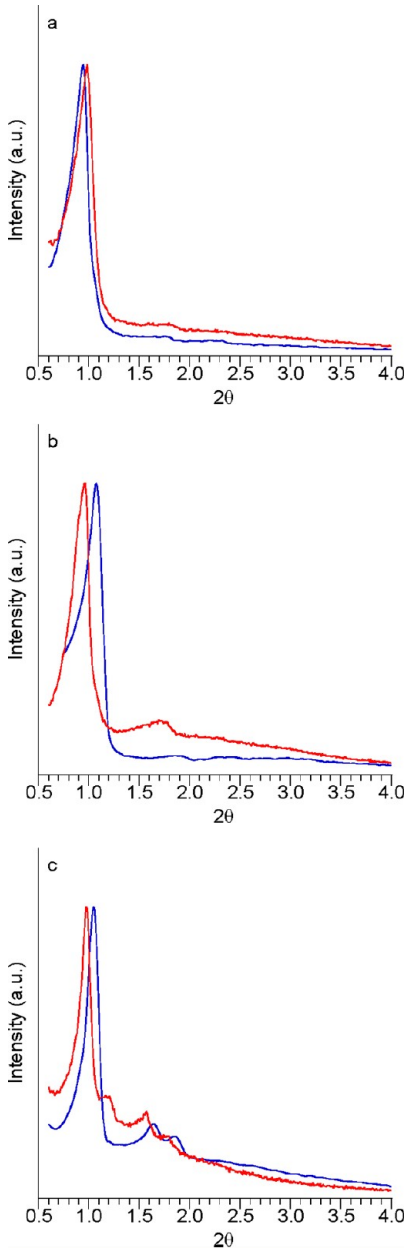

Figure 3. XRD reflection patterns for pSO_3H-SBA-15 catalysts: (a) E90; (b) E45; and (c) E0, before use in the dehydration reaction (blue) and after use on-stream (red) at 403 K. E90, E45, and E0 were on-stream for 60, 51, and 55 h, respectively.

reflection was also observed at 1.86° (Figure 3c). The observation of d_{110} and d_{200} reflections indicates a long-range, quasi-crystalline arrangement of the mesopores. Incorporation of propylsulfonic acid groups was confirmed by ^{13}C CP/MAS NMR and quantified by sulfur analysis. Recently, we reported that oxidation of MPTMS to the corresponding sulfonic acid by H_2O_2 added during SBA-15 synthesis is quantitative, according to XPS.[36] Furthermore, the results of acid−base titration on those materials were consistent with the S analysis. Thus, we are confident that the sulfur analysis correctly reflects the propylsulfonic acid content. For E0, E45, E90, and pSO_3H-SC, the propylsulfonic acid loadings are 1.10, 0.71, 0.53, and 0.65 mmol/g, respectively, corresponding to acid densities of 1.89, 1.27, 0.97, and 0.98 μmol/m^2, respectively. For E90 and E45, signals characteristic of framework ethane derived from the condensation of BTME were observed in both the ^{13}C CP/MAS and ^{29}Si MAS NMR spectra. Particle morphology, surface texture, and pore ordering were also characterized by SEM. E90 consists of fused chains of deformed spheres, each ~1 μm in diameter (Figure 4a). At a higher magnification, hexagonally

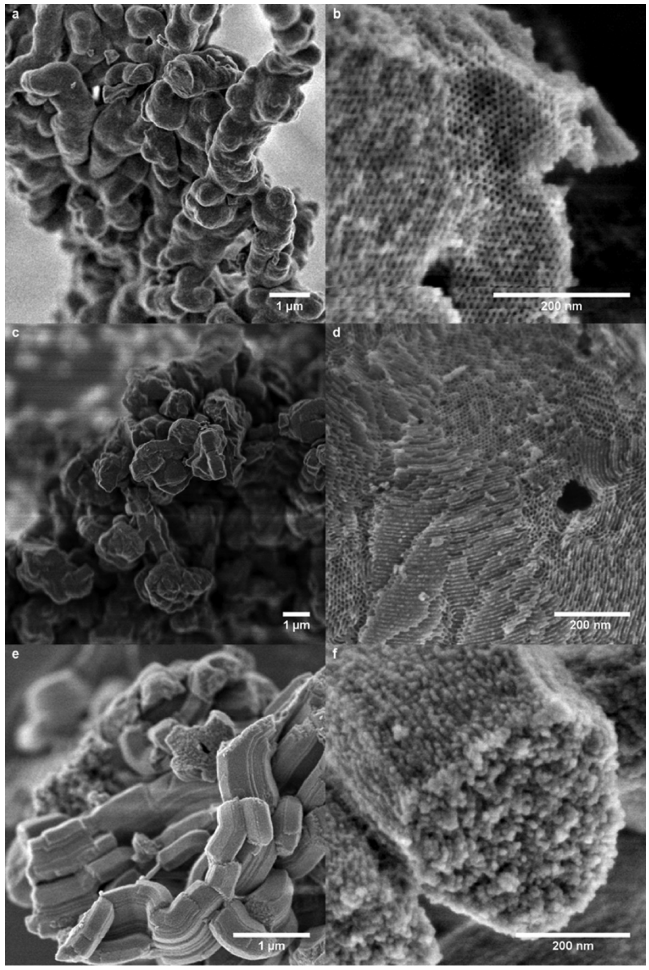

Figure 4. SEM images of fresh pSO_3H-SBA-15 catalysts at two different magnifications for (a, b) E90, (c, d) E45, and (e, f) E0.

arranged pores are visible on the particle surface (Figure 4b). In contrast, the particles of E45 are faceted and range from 1 to 3 μm in diameter and from 0.5 to 1 μm in thickness (Figure 4c). The primary particles also appear to be aggregated or fused into larger clusters. Similar to E90, hexagonal arrays of pores and channels are visible on the particle surface (Figure 4d). E0 consists of clusters of deformed, hexagonally shaped particles (Figure 4e); however, at higher magnifications, the pore entrances are obscured (Figure 4f). This is likely due to sample charging.[47] The effect may be reduced for E90 and E45 by the presence of carbon within the framework.[48,49]

Catalytic Dehydration of Fructose. To achieve efficient mixing in the packed-bed reactor, a single-phase reaction solvent was required. The solvent chosen for this study was a 4:1 mixture of THF/water, which was observed visually to be single-phase both at room temperature and under the reaction conditions (i.e., at 403 K, in the absence of salt). Water is required to solubilize the fructose, and the use of THF as cosolvent leads to higher selectivity for HMF. The organic solvent is readily separated from the product mixture because of

dx.doi.org/10.1021/cs300303v | ACS Catal. 2012, 2, 1865−1876

its high volatility. Each solid acid catalyst was loaded separately into the 1/4 in. simple packed-bed reactor to study its reactivity in the dehydration of fructose to HMF. Preliminary batch reactions (see Supporting Information) were used to determine the weight loadings of catalyst needed to achieve similar, high fructose conversions in each case. The reactor bed length varied from about 1.5 to 4.0 in., depending on the acid site density and bulk density of each catalyst. The HMF selectivity, the fructose conversion, and the rate of HMF production, monitored as a function of time on-stream, are shown in Figures 5 and 6.

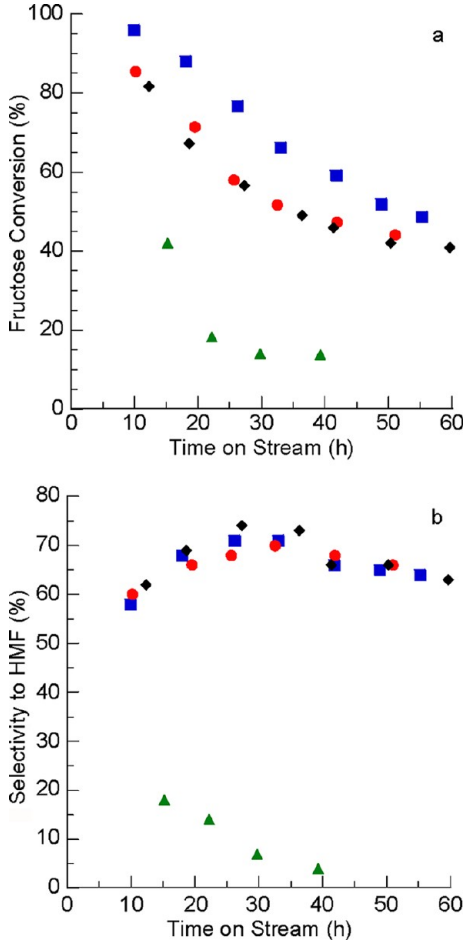

Figure 5. Fructose conversion (a) and HMF selectivity (b) as a function of time on-stream in the 1/4 in. simple reactor at 403 K for the various pSO_3H-SBA-15 catalysts: E0 (blue squares), E45 (red circles), and E90 (black diamonds), as well as pSO_3H-SC (green triangles). The flow rate was constant at 0.14 mL/min.

For the ordered mesoporous catalysts E0, E45 and E90, initial fructose conversion was >80% (Figure 5a). Selectivity stabilized between 65 and 75% after ∼24 h on stream, then decreased slightly at longer times. For the nonordered pSO_3H-SC catalyst, the initial fructose conversion was 42%. HMF selectivity was low and decreased sharply over the course of the reaction. This catalyst also showed the greatest extent of deactivation, losing 94% of its activity over 24 h (Figure 6). By comparison, all of the ordered mesoporous catalysts (E0, E45, and E90) showed much higher stabilities. Although differences in the deactivation rates of the ordered materials were not obvious using this reactor configuration, all of them do deactivate to some extent (vide infra).

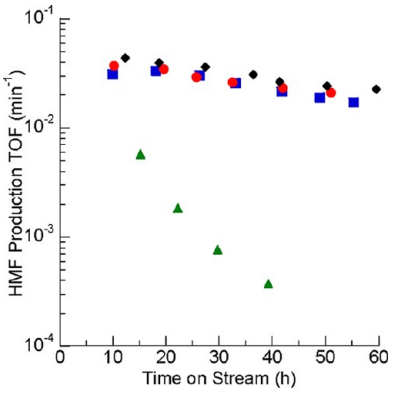

Figure 6. Rate of HMF production as TOF (min^{-1}) in the 1/4 in. simple reactor at 403 K as a function of time on-stream for various pSO_3H-SBA-15 catalysts: E0 (blue squares), E45 (red circles), and E90 (black diamonds), as well as pSO_3H-SC (green triangles). The flow rate was constant at 0.14 mL/min.

Postreaction Catalyst Characterization. To investigate the deactivation mechanism(s), the catalysts were recovered after 39−60 h of operation in the flow reactor. The pSO_3H-SC catalyst was also characterized by ^{13}C CP/MAS and ^{29}Si MAS NMR (Figure 7). Its ^{13}C spectrum, like that of pSO_3H-SBA-

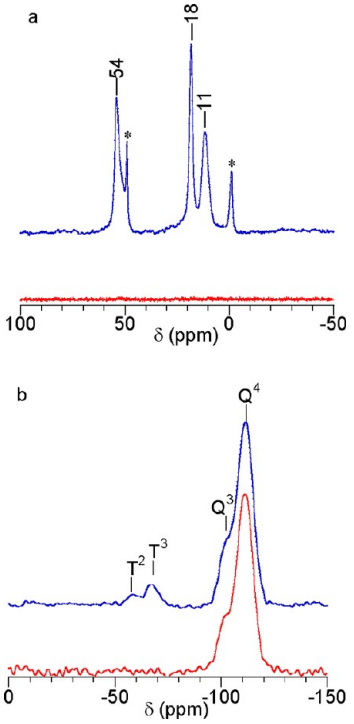

Figure 7. Solid-state NMR spectra of pSO_3H-SC catalyst, as-received from Silicycle (blue) and after 39 h on-stream at 403 K (red): (a) ^{13}C CP/MAS NMR and (b) ^{29}Si MAS NMR. Spinning rate, 10 kHz.

15,[38] contains three signals (11, 18, 54 ppm) representing the anchored propylsulfonic acid groups. Two additional signals at 0 and 50 ppm are attributed to methyl ($SiCH_3$) and methoxy ($SiOCH_3$) groups, respectively. The connectivity of the various silicon sites is specified using the ^{29}Si NMR descriptors T^n and Q^n, where n is the number of siloxane bonds linking the Si site to the silica framework. T^n is used for [SiR] groups with one covalent bond to carbon and up to three siloxane bonds, and

dx.doi.org/10.1021/cs300303v | ACS Catal. 2012, 2, 1865−1876

Q^n sites possess no Si−C bonds. In the ^{29}Si CP/MAS NMR spectrum of pSO_3H-SC, signals for both T^2 and T^3 sites, corresponding to two different anchored propylsulfonic acid sites, are visible. Incomplete condensation of MPTMS leading to T^2 sites is consistent with the observation of $[SiOCH_3]$ groups (due to incomplete silane condensation) in the ^{13}C CP/MAS NMR spectrum. The origin of the $[SiCH_3]$ sites is unknown, since the commercial material is described as "not end-capped".

The ^{13}C CP/MAS NMR spectrum of used pSO_3H-SC-H contains no peaks (Figure 7a), indicating that virtually all of the propylsulfonic acid groups had been removed. Similarly, the ^{29}Si MAS NMR spectrum shows a complete loss of T^n sites (Figure 7b). The propylsulfonic acid groups on pSO3H-SC are therefore deemed highly susceptible to leaching. In contrast, for the SBA-15-type materials, the signals attributed to propylsulfonic acid groups (11, 18, 54 ppm) in the ^{13}C CP/MAS spectra are merely attenuated compared with their intensities prior to use (Figure 8). Unexpectedly, signals for ethoxy groups present in the E90 and E45 catalysts prior to reaction are still visible at 16 and 59 ppm. These ethoxy groups are likely associated with uncondensed silanes that are inaccessible, being located within the framework.

No new signals were detected in the ^{13}C CP/MAS NMR spectra of the PMO catalysts after use, indicating little adsorption of products on the catalyst. Several weak signals in the ^{13}C CP/MAS NMR spectrum of the used E0 catalyst are attributed to physisorbed solvent due to incomplete drying (Figure 8c). Postreaction, the ^{29}Si CP/MAS NMR spectrum of the E0 catalyst shows a significant decrease in the T^n/Q^n ratio, indicating a loss of functional groups (Figure 9); however, it is not possible to assess functional group loading or reorganization of the framework in the same way for the E90 and E45 catalysts because T^2 and T^3 signals from the bridging ethane groups of the PMO framework obscure the signals of the anchored acid sites for both the fresh and used materials.

The powder XRD patterns and N_2 sorption isotherms confirm that all catalysts undergo changes in framework structure during ∼50 h of reactor operation. The surface area of pSO_3H-SC declines by 57%. This suggests significant restructuring of the nonordered framework of pSO_3H-SC under reaction conditions. Of the ordered catalysts, the differences are greatest for E0, and least for E90. Each material retains its *p6mm* mesoporous framework, as indicated by persistence of the d_{100} reflection in the powder XRD (Figure 3). The corresponding N_2 sorption isotherms remain type IV (Figure 2). For E90, the surface area, pore size, pore volume, and pore diameter distribution remain relatively unchanged during use (Table 1 and Figure 10a). Similarly, only minor changes are observed in the powder XRD pattern for E90 (Figure 3a). For E45, exposure to reaction conditions causes the mesopore volume to increase, while the micropore volume decreases significantly due the collapse of interpore microchannels.[50] As a result, the surface area increases by 8% after reaction, and the distribution of pore diameters broadens slightly (Figure 10b). However, these physicochemical changes do not result in significant changes to the mesostructure as shown by XRD (Figure 3b).

The structural alterations to E0 induced under the reaction conditions are significant relative to those detected for the PMO catalysts. E0 undergoes a loss of surface area (16%), accompanied by an increase in pore volume from 0.63 to 1.2 $cm^3\ g^{-1}$. The average pore size also increases by ca. 1 nm, to 6.8 nm (Table 1). The pore diameter distribution broadens significantly during use (Figure 10c). While the powder XRD pattern still shows the d_{100}, d_{110}, and d_{200} reflections typical of

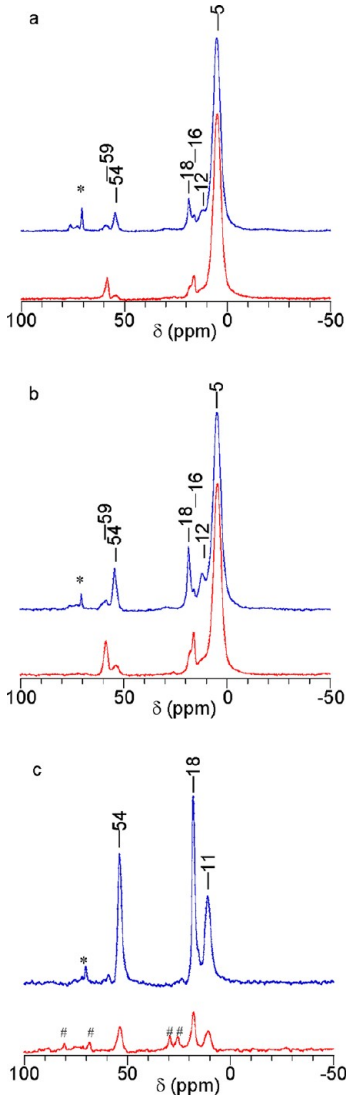

Figure 8. Solid-state ^{13}C CP/MAS NMR spectra of various pSO_3H-SBA-15 catalysts before (blue) and after (red) use on-stream at 403 K: (a) E90, (b) E45, and (c) E0. E90, E45, and E0 were on-stream for 60, 51, and 55 h, respectively. Spinning rate, 10 kHz. The asterisk (*) indicates residual surfactant signals; the pound sign (#) indicates physisorbed solvent signals.

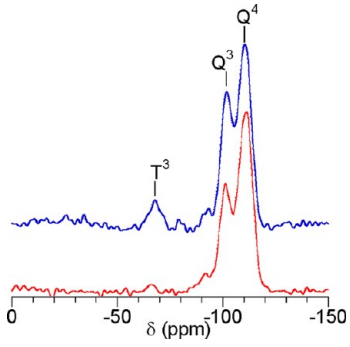

Figure 9. Solid-state ^{29}Si MAS NMR spectra of E0 before (blue) and after (red) use on-stream at 403 K for 55 h. Spinning rate, 10 kHz.

dx.doi.org/10.1021/cs300303v | *ACS Catal.* 2012, 2, 1865−1876

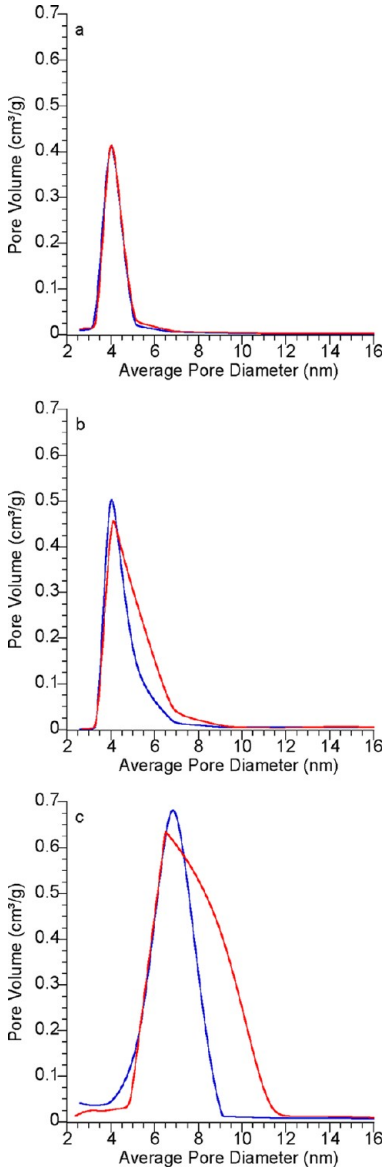

Figure 10. Pore size distribution curves for various pSO_3H-SBA-15 catalysts: (a) E90, (b) E45, and (c) E0 before (blue) and after (red) use on-stream at 403 K. E90, E45, and E0 were on-stream for 60, 51, and 55 h, respectively.

an SBA-15-type material, the relative intensities of the d_{110} and d_{200} reflections has decreased, indicating a loss of long-range *p6mm* pore ordering (Figure 3c). A new reflection also appears on the shoulder of the d_{100} reflection, suggesting that the periodicity of the mesostructure has changed somewhat under reaction conditions.

To ensure that changes in the framework order were detectable by imaging, the operating time for each SBA-15-type catalyst was prolonged to 148−190 h (see Supporting Information). All three recovered catalysts appeared to retain their basic morphological characteristics as observed by SEM (Figure 11a,c,e). At higher magnification, the *p6mm* arrangement of pores is still clearly visible for E90 and E45 (Figure 11b,d); however, the ridges observed on the surface of the fresh E0 catalyst (Figure 4f) were destroyed during extended operation (Figure 11f). In the TEM, the images of E90 (Figure 12b) and E45 (Figure 12d) after operation also show hexagonally arranged mesopores; however, the channels that

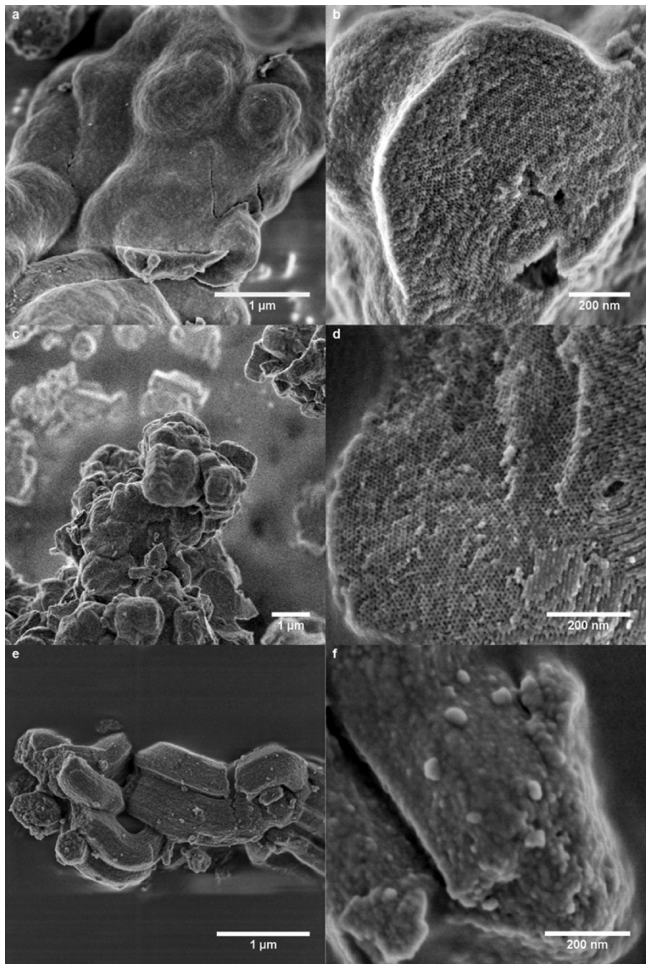

Figure 11. SEM images of various pSO_3H-SBA-15 catalysts after operation in a flow reactor at 403 K for E90 (a,b), E45 (c,d), and E0 (e,f). E90, E45, and E0 were on-stream for 148, 190, and 166 h, respectively (see Supporting Information).

were apparent for E0 in Figure 12e are barely visible by TEM after extended use (Figure 12f). Thus, the structural integrity of the ordered mesoporous silica (E0) is severely compromised under reaction conditions, while the more robust structures of the PMOs are largely maintained.

Postreaction characterization of each ordered mesoporous support indicated that the mesopores remain unobstructed: no humin signals were observed by solid-state ^{13}C CP/MAS NMR. Consequently, the deactivation that occurs under reaction conditions (Figure 5a and 6) appears to be largely the result of acid site cleavage. According to elemental analysis, the S/Si ratios decreased by 64, 71, and 85% for E90, E45, and E0, respectively, relative to the initial values. To confirm this hypothesis, E90 and pSO_3H-SC were stirred overnight in D_2O at 403 K, and the filtrates were analyzed using solution-state ^1H NMR. Signals at 0.812 (t), 1.881 (quin), and 2.967(t) ppm were detected for both materials, representing the methylene protons of 3-(trideuteroxysilyl)-1-propanesulfonic acid (eq 1):

$$(\equiv SiO)_3Si(CH_2)_3SO_3D + 3D_2O \rightarrow 3\equiv SiOD + (DO)_3Si(CH_2)_3SO_3D \quad (1)$$

This result suggests that loss of propylsulfonic acid groups occurs in all catalysts under reaction conditions, although the anchored sites are more stable on the PMOs (E90 and E45)

dx.doi.org/10.1021/cs300303v | *ACS Catal.* 2012, 2, 1865−1876

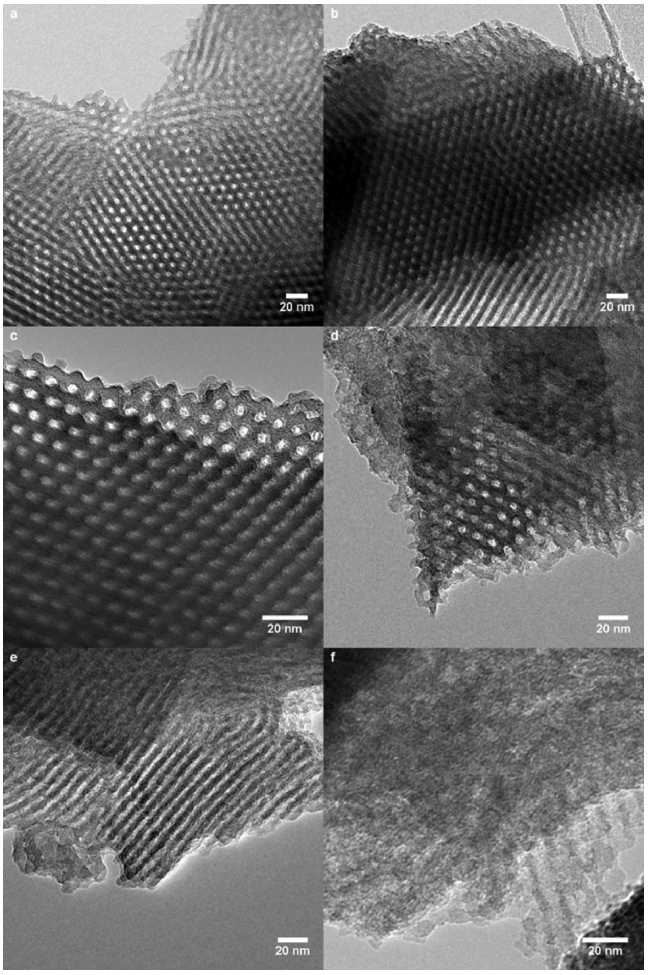

Figure 12. TEM images of various pSO_3H-SBA-15 catalysts, before (left), and after (right) operation in a flow reactor at 403 K, for E90 (a,b), E45 (c,d), and E0 (e,f). E90, E45, and E0 were on-stream for 148, 190, and 166 h, respectively (see Supporting Information).

than on the purely siliceous frameworks (E0 and pSO_3H-SC). Interestingly, the significant loss of acid sites inferred from the elemental analysis is not consistent with the low apparent rates of deactivation for the mesoporous ordered materials (Figure 6). However, we will show that the latter is an artifact of the reactor design (vide infra).

Quantitative Comparison of Catalyst Deactivation Rates. The catalyst bed was shortened by increasing the reactor diameter to 1/2 in. and decreasing the catalyst mass, from ~300 mg to ≤50 mg. Decreasing the bed length results in a lower pressure drop and a decreased driving force for liquid channeling. In addition, the WHSV was increased to lower the conversion, in order to study catalyst activity in the kinetic regime. Decreasing the conversion will also limit the effect, if any, of liquid channeling. After implementing these changes, the rate of HMF production became independent of linear velocity at constant WHSV (see Supporting Information).

The results obtained using this reactor design and a constant molar loading of catalyst are shown in Figure 12 and Table 2. At 403 K, the initial fructose conversions were 6, 15, 28, and 11% for E0, E45, E90 and pSO_3H-SC, respectively, and the selectivities were 68, 52, 43, and 26% for the same catalysts. The initial TOFs (measured under steady-state conditions) increase with the extent of incorporation of ethane groups into the silica framework. Thus E90 possesses the highest initial TOF (0.091 min^{-1}), followed by E45 (0.056 min^{-1}), E0 (0.031 min^{-1}), and pSO_3H-SC (0.021 min^{-1}).

Table 2. Comparison of First-Order Deactivation Rate Constants Measured in the 1/2 in. Reactor, without and with Added Silica Gel

catalyst	catalyst only, h^{-1}	catalyst + silica gel, h^{-1}
pSO_3H-SC	0.152	0.065
E0	0.124	0.027
E45	0.032	0.012
E90	0.053	0.022

Large stability differences between the catalysts, particularly the mesoporous catalysts, become apparent with the shorter catalyst bed. Although the E0 catalyst is the least stable of the ordered mesoporous catalysts, it is, nevertheless, more stable than the nonordered pSO_3H-SC catalyst. As evidenced by the postreaction characterization, the structural order of E0 is largely maintained for nearly 60 h on-stream, whereas pSO3H-SC loses all of its acid sites and a significant fraction of its prereaction surface area. Previously, we showed that grafted acid sites in nonordered silicas are less stable than acid sites incorporated through co-condensation in ordered silicas.[35] The lower stability was ascribed to attachment of the propylsulfonic acid sites via fewer siloxane linkages. Interestingly, the ^{29}Si MAS NMR spectrum shows that the acid sites in the nonordered pSO_3H-SC and E0 have similar siloxane attachments, yet the former is still much less stable. Therefore the 2-D hexagonal mesopore ordering appears to be correlated with higher catalyst stability. The incorporation of ethane groups into silica framework further increases catalyst stability, as evidenced by the significantly lower first-order deactivation rate constants for E45 and E90. The increased stability of the organosilicas is likely a consequence of the hydrophobic microenvironment, which reduces the local water concentration and, therefore, acid site hydrolysis.

Mitigating Catalyst Deactivation. In Figure 6, the leveling of the deactivation rates may be an artifact of readsorption of cleaved acid functional groups in the long catalyst bed. It has been reported that 3-(trihydroxysilyl)-1-propanesulfonic acid can be attached to a silica surface (eq 2) by mild heating.[51]

$$n(\equiv\mathrm{SiOH}) + \mathrm{RSi(OH)_3} \rightarrow (\equiv\mathrm{SiO})_n\mathrm{SiR(OH)_{3-}}_n + n\mathrm{H_2O} \quad (2)$$

To evaluate the potential for acid readsorption under flow conditions, both silica gel (122 mg) and catalyst (in appropriate amounts, each corresponding to 26.6 μmol of propylsulfonic acid groups) were loaded into the 1/2 in. diameter reactor, creating the stacked bed shown in Figure 14. The silica gel itself is almost inactive for the production of HMF: in a batch reaction using silica gel as the catalyst, HMF was produced at a rate of less than 0.01 μmol min^{-1} (g SiO_2)$^{-1}$.

Reactivity studies were conducted using reaction conditions identical to those employed previously with the 1/2 in. diameter reactor (Figure 13a); the results are shown in Figure 13b. The decrease in the pseudo-first-order deactivation rate constants (Table 2) demonstrates that the presence of the silica gel slows catalyst deactivation. When stacked with silica gel, E45 again yielded the lowest deactivation rate constant (0.012 h^{-1}). For pSO_3H-SC, the observed deactivation rate constant

dx.doi.org/10.1021/cs300303v | ACS Catal. 2012, 2, 1865−1876

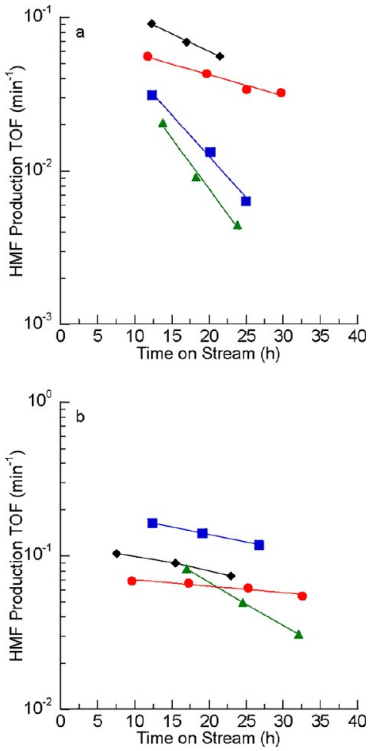

Figure 13. Rates of HMF production (TOF) as a function of time on-stream in (a) the 1/2 in. diameter simple packed bed reactor, and (b) the 1/2 in. diameter stacked bed reactor with 0.122 g silica gel, both at 403 K, using catalysts pSO_3H-SC (40 mg, green triangles), E0 (25 mg, blue squares), E45 (39 mg, red circles), and E90 (50 mg, black diamonds). Each catalyst mass corresponds to a total acid content of 26.6 μmol. The flow rate was constant at 0.17 mL/min.

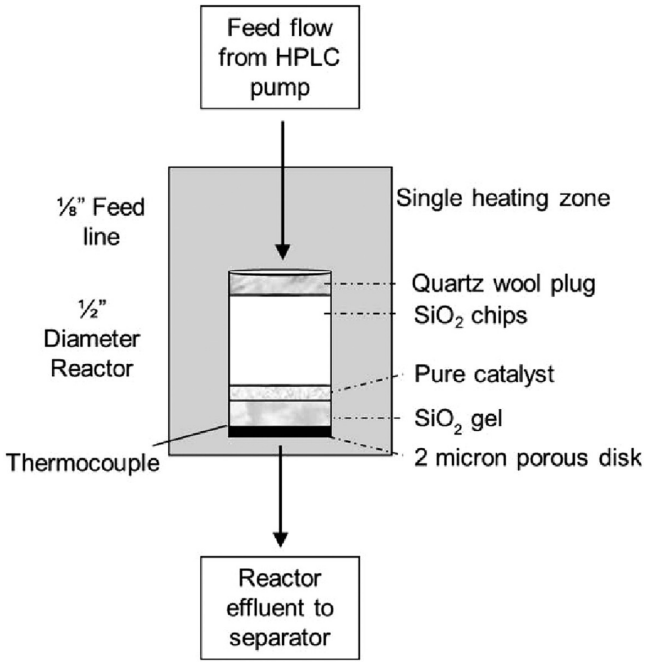

Figure 14. Schematic representation of the 1/2-in.-diameter stacked bed reactor loaded with silica gel above the catalyst layer. The stacked bed is supported by a porous glass disk.

decreased by 57% (a factor of 2.3) in the presence of the silica gel; however, it is still twice that of E45 alone. The deactivation rate constants for both E90 and E0 stacked with silica gel (0.022 and 0.027 h^{-1}, respectively) are slightly lower than for E45 alone (0.032 h^{-1}). Overall, the deactivation rate constant for E0 decreased the most in the presence of the silica gel (a factor of 4.6).

The effect of the stacked-bed configuration is even more dramatic for pSO_3H-SC in the 1/4 in. diameter reactor (Figure 15). The rate of HMF formation remained nearly constant for

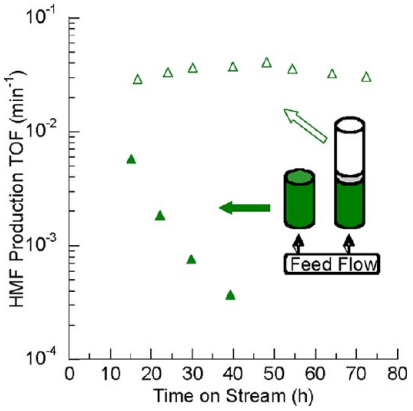

Figure 15. Rate of HMF production (TOF) as a function of the time on-stream in both 1/4 in. reactors for pSO_3H-SC alone (solid green triangles) and in a stacked bed with silica gel (hollow green triangles). In both experiments, 330 mg of pSO_3H-SC (0.215 mmol acid) was used. In the stacked bed experiment, 812 mg of silica gel was also used. Inset: Schematic of catalyst bed with pSO_3H-SC (green), quartz wool (gray), and silica gel (white); feed enters at the bottom of the reactor and exits at the top.

60 h, compared with a pSO_3H-SC-only bed, which experienced nearly complete deactivation under the same reaction conditions (similar to the results shown in Figure 6). The pseudo-first-order deactivation rate constant is ~5 times slower than for Silicycle pSO_3H-SC alone, and a factor of 2 slower than that observed with the stacked bed in the 1/2 in. reactor. This result illustrates the importance of reactor configuration on deactivation for these types of catalyst. Readsorption of cleaved acid sites is more significant in the longer reactor bed, and when silica gel is present.

The apparent increased stability of the anchored acid catalysts in the presence of silica gel is evidence for readsorption of the leached 3-(trihydroxysilyl)-1-propanesulfonic acid by the silica gel. For confirmation, the silica gel layer (stacked with pSO_3H-SC in the 1/4 in. diameter reactor) was recovered and characterized by solid-state NMR (Figure 16). The signals at 9, 17, and 54 ppm in the ^{13}C CP/MAS NMR spectrum are consistent with the presence of anchored propylsulfonic groups. Additional signals at 25 and 68 ppm are due to residual THF. Most importantly, T^n sites are detected by ^{29}Si CP/MAS NMR. The spectrum in Figure 16b confirms that the acid groups are covalently bonded to the silica gel through siloxane bonds, rather than physisorbed on the surface.

Although the anchored acid sites in the PMO catalysts are more stable toward leaching relative to catalysts with purely siliceous frameworks, surface hydroxyls located in the hydrophobic pore channels may still promote readsorption of the trihydroxysilane, resulting in slower deactivation. The difference in stabilities of E90 and E45 suggest that it may be possible to optimize the hydroxyl content of the PMO further via its

dx.doi.org/10.1021/cs300303v | ACS Catal. 2012, 2, 1865−1876

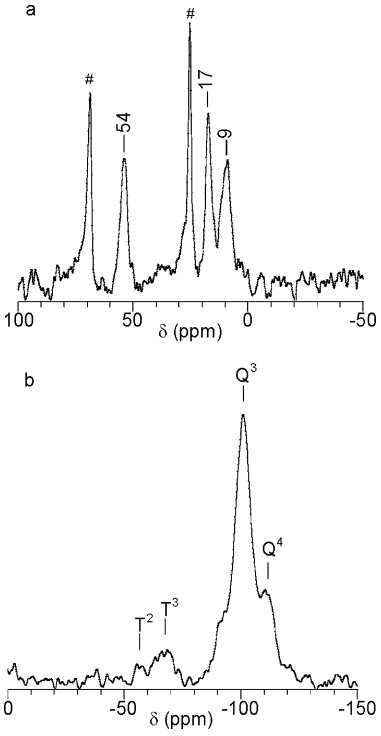

Figure 16. Solid-state NMR spectra of silica gel after use in a stacked bed reactor for 70 h at 403 K: (a) ^{13}C CP/MAS NMR and (b) ^{29}Si CP/MAS NMR. Spinning rate, 10 kHz.

composition (i.e., the TMOS/BTME synthesis ratio) to slow deactivation even more.

CONCLUSIONS

Two ethane-containing PMO-based propylsulfonic acids catalysts were synthesized, and their activity, selectivity, and stability in the dehydration of fructose were compared with a commercial silica-supported propylsulfonic acid and an SBA-15-supported propylsulfonic acid catalyst. The catalysts with ordered pore structures are more selective and more robust. With an appropriate reactor configuration, a quantitative comparison of stability for the propylsulfonic acid catalysts was possible, and the intrinsic stability of the organosilica catalysts was evident. For all catalysts, the primary deactivation mechanism is hydrolytic cleavage of the acid sites. Analysis of the deactivation rate was complicated by readsorption of the cleaved acid. Cleavage is reversible, and the observed deactivation rate can be reduced by stacking a bed of silica gel after the propylsulfonic acid catalyst.

ASSOCIATED CONTENT

Supporting Information

Additional characterization for E90, E45, and E0 materials by N_2 adsorption/desorption, XRD, and solid-state CP-MAS NMR (^{13}C and ^{29}Si) as well as details of the linear velocity study. This material is available free of charge via the Internet at http://pubs.acs.org.

AUTHOR INFORMATION

Corresponding Author

*E-mails: (J.A.D.) dumesic@engr.wisc.edu, (S.L.S.) sscott@engineering.ucsb.edu.

Author Contributions

[‖]The first two authors contributed equally to this work.

Notes

The authors declare no competing financial interest.

ACKNOWLEDGMENTS

The authors thank Dr. Huang Kai and Dr. Mu-Tong Niu of the Suzhou Institute of Nano-Tech and Nano-Bionics for assistance in collecting the SEM images and Thomas J. Schwartz of UW–Madison for assistance in collecting the solution-state NMR spectra. This work was supported by the NSF under the auspices of the Center for Enabling New Technologies through Catalysis (CENTC). A.J.C. acknowledges the PIRE-ECCI (NSF Grant OISE-0530268) for a fellowship. Portions of this work made use of facilities of the Materials Research Laboratory, supported by the MRSEC Program of the National Science Foundation under Award No. DMR05-20415.

REFERENCES

(1) Werpy, T.; Petersen, G. *Top Value Added Chemicals from Biomass*; National Renewable Energy Laboratory: Golden, CO; 2004; Vol 1.
(2) Davis, S. E.; Houk, L. R.; Tamargo, E. C.; Datye, A. K.; Davis, R. J. *Catal. Today* **2011**, *160*, 55.
(3) Moreau, C.; Belgacem, M. N.; Gandini, A. *Top. Catal.* **2004**, *27*, 11.
(4) Sanborn, A. J.; Bloom, P. D. Preparation of 5-bis-(hydroxymethyl)furaldehyde derivatives for use in various areas. US Patent US7393963B2, 2008.
(5) Faber, M. Adipic acid from biomass. US Patent US4400468A, 1983.
(6) Chia, M.; Pagán-Torres, Y. J.; Hibbitts, D.; Tan, Q.; Pham, H. N.; Datye, A. K.; Neurock, M.; Davis, R. J.; Dumesic, J. A. *J. Am. Chem. Soc.* **2011**, *133*, 12675.
(7) Koso, S.; Ueda, N.; Shinmi, Y.; Okumura, K.; Kizuka, T.; Tomishige, K. *J. Catal.* **2009**, *267*, 89.
(8) Nakagawa, Y.; Tomishige, K. *Catal. Commun.* **2010**, *12*, 154.
(9) Utne, T.; Jones, R. E.; Garber, J. D. 1,6-Hexanediol. US Patent US3070633, 1962.
(10) Tong, X.; Ma, Y.; Li, Y. *Appl. Catal., A* **2010**, *385*, 1.
(11) Gong, W. H. Production of terephthalic acid from 2,5-furandicarboxylate. US Patent WO2009064515A1, 2009.
(12) Safo, M. K.; Abdulmalik, O.; Danso-Danquah, R.; Burnett, J. C.; Nokuri, S.; Joshi, G. S.; Musayev, F. N.; Asakura, T.; Abraham, D. J. *J. Med. Chem.* **2004**, *47*, 4665.
(13) Huber, G. W.; Chheda, J. N.; Barrett, C. J.; Dumesic, J. A. *Science* **2005**, *308*, 1446.
(14) West, R. M.; Tucker, M. H.; Braden, D. J.; Dumesic, J. A. *Catal. Commun.* **2009**, *10*, 1743.
(15) Roman-Leshkov, Y.; Barrett, C. J.; Liu, Z. Y.; Dumesic, J. A. *Nature* **2007**, *447*, 982.
(16) Kuster, B. F. M. *Starch-Starke* **1990**, *42*, 314.
(17) Bicker, M.; Kaiser, D.; Ott, L.; Vogel, H. J. *Supercrit. Fluids* **2005**, *36*, 118.
(18) Moreau, C.; Finiels, A.; Vanoye, L. *J. Mol. Catal., A: Chem.* **2006**, *253*, 165.
(19) Zhao, H. B.; Holladay, J. E.; Brown, H.; Zhang, Z. C. *Science* **2007**, *316*, 1597.
(20) Zakrzewska, M. E.; Bogel-Łukasik, E.; Bogel-Łukasik, R. *Chem. Rev.* **2010**, *111*, 397.
(21) Qi, X.; Watanabe, M.; Aida, T. M.; Smith, J. R. L. *Green Chem.* **2008**, *10*, 799.
(22) Shimizu, K.-I.; Uozumi, R.; Satsuma, A. *Catal. Commun.* **2009**, *10*, 1849.
(23) Kazi, F. K.; Patel, A. D.; Serrano-Ruiz, J. C.; Dumesic, J. A.; Anex, R. P. *Chem. Eng. J.* **2011**, *169*, 329.
(24) Lewkowski, J. *ARKIVOC* **2001**, *2*, 17.

(25) Mercadier, D.; Rigal, L.; Gaset, A.; Gorrichon, J.-P. *J. Chem. Technol. Biotechnol.* **1981**, *31*, 489.
(26) Chheda, J. N.; Roman-Leshkov, Y.; Dumesic, J. A. *Green Chem.* **2007**, *9*, 342.
(27) Roman-Leshkov, Y.; Chheda, J. N.; Dumesic, J. A. *Science* **2006**, *312*, 1933.
(28) Román-Leshkov, Y.; Dumesic, J. *Top. Catal.* **2009**, *52*, 297.
(29) McNeff, C. V.; Nowlan, D. T.; McNeff, L. C.; Yan, B.; Fedie, R. L. *Appl. Catal., A: Gen.* **2010**, *384*, 65.
(30) Rivalier, P.; Duhamet, J.; Moreau, C.; Durand, R. *Catal. Today* **1995**, *24*, 165.
(31) Moreau, C.; Durand, R.; Razigade, S.; Duhamet, J.; Faugeras, P.; Rivalier, P.; Ros, P.; Avignon, G. *Appl. Catal., A: Gen.* **1996**, *145*, 211.
(32) Carniti, P.; Gervasini, A.; Biella, S.; Auroux, A. *Catal. Today* **2006**, *118*, 373.
(33) Carniti, P.; Gervasini, A.; Marzo, M. *Catal. Today* **2010**, *152*, 42.
(34) Nakamura, Y.; Morikawa, S. *Bull. Chem. Soc. Jpn.* **1980**, *53*, 3705.
(35) Crisci, A. J.; Tucker, M. H.; Dumesic, J. A.; Scott, S. L. *Top. Catal.* **2010**, *53*, 1185.
(36) Crisci, A. J.; Tucker, M. H.; Lee, M.-Y.; Jang, S. G.; Dumesic, J. A.; Scott, S. L. *ACS Catal.* **2011**, *1*, 719.
(37) Miao, S.; Shanks, B. H. *Appl. Catal., A: Gen.* **2009**, *359*, 113.
(38) Margolese, D.; Melero, J. A.; Christiansen, S. C.; Chmelka, B. F.; Stucky, G. D. *Chem. Mater.* **2000**, *12*, 2448.
(39) Dias, A. S.; Pillinger, M.; Valente, A. A. *J. Catal.* **2005**, *229*, 414.
(40) Liu, J.; Yang, Q.; Kapoor, M. P.; Setoyama, N.; Inagaki, S.; Yang, J.; Zhang, L. *J. Phys. Chem. B* **2005**, *109*, 12250.
(41) Wang, W.; Lofgreen, J. E.; Ozin, G. A. *Small* **2010**, *6*, 2634.
(42) Burleigh, M. C.; Markowitz, M. A.; Jayasundera, S.; Spector, M. S.; Thomas, C. W.; Gaber, B. P. *J. Phys. Chem. B* **2003**, *107*, 12628.
(43) Yang, Q.; Liu, J.; Zhang, L.; Li, C. *J. Mater. Chem.* **2009**, *19*, 1945.
(44) Hoffmann, F.; Cornelius, M.; Morell, J.; Fröba, M. *Angew. Chem., Int. Ed.* **2006**, *45*, 3216.
(45) Yang, Q.; Liu, J.; Yang, J.; Kapoor, M. P.; Inagaki, S.; Li, C. *J. Catal.* **2004**, *228*, 265.
(46) Rác, B.; Hegyes, P.; Forgo, P.; Molnár, Á. *Appl. Catal., A: Gen.* **2006**, *299*, 193.
(47) Che, S.; Lund, K.; Tatsumi, T.; Iijima, S.; Joo, S. H.; Ryoo, R.; Terasaki, O. *Angew. Chem., Int. Ed.* **2003**, *42*, 2182.
(48) Wang, W.; Grozea, D.; Kohli, S.; Perovic, D. D.; Ozin, G. A. *ACS Nano* **2011**, *5*, 1267.
(49) Gray, P. R.; Hurst, P. J.; Lewis, S. H.; Meyer, R. G. *Analysis and Design of Analog Integrated Circuits*; 5th ed.; Wiley: New York, 2009.
(50) Zhang, F.; Yan, Y.; Yang, H.; Meng, Y.; Yu, C.; Tu, B.; Zhao, D. *J. Phys. Chem. B* **2005**, *109*, 8723.
(51) Jespersen, M. L.; Mirau, P. A.; Von Meerwall, E.; Vaia, R. A.; Rodriguez, R.; Giannelis, E. P. *ACS Nano* **2010**, *4*, 3735.